JOURNAL OF MATERIALS SCIENCE 24 (1989) 3779–3786

Precipitation in liquid-quenched Al–Mg alloys; a study using X-ray diffraction line shift and line broadening

P. VAN MOURIK, N. M. MAASWINKEL, Th. H. DE KEIJSER, E. J. MITTEMEIJER
Laboratory of Metallurgy, Delft University of Technology, Rotterdamseweg 137, 2628 AL Delft, The Netherlands

The precipitation process in liquid-quenched alloys of aluminium with 3.2, 10.5 and 16.7 at% Mg on ageing at 404, 450 and 492 K was investigated by X-ray diffraction analysis. It was found that only β'-phase precipitation occurred. During ageing, the average aluminium-matrix lattice parameter was determined from the line position, while a measure for the lattice spacing variations was deduced from line broadening. The β'-phase precipitation was found to occur inhomogeneously; for one alloy, splitting of diffraction lines was observed. The (asymmetrical) line-broadening changes observed during the β'-phase precipitation could consistently be conceived as dominated by the inhomogeneous nature of the β'-phase precipitation process. The (symmetrical) line broadening retained after completed precipitation was ascribed to the volume misfit between the precipitated β'-phase particles and the aluminium-matrix. Analysis of the aluminium-matrix lattice parameter changes with ageing time revealed that the β'-phase precipitation rate is governed by the magnesium volume diffusion.

1. Introduction

The initially high cooling/solidification rate inherent to liquid quenching, i.e. rapid quenching from the liquid state, can highly influence the kinetics of precipitation in aluminium base alloys. Liquid quenching (LQ), compared to solid quenching (SQ), can result in an increased amount of excess vacancies and an enhanced degree of solute supersaturation. This has been demonstrated by experiments with AlSi alloys [1].

Only a few data exist about the precipitation phenomena in LQ AlMg alloys [2], whereas the ageing phenomena in conventionally produced SQ AlMg alloys were the subject of several previous studies [3–16].

In AlSi alloys, precipitation directly results in the equilibrium phase of (practically) pure silicon, whereas the precipitation in quenched AlMg alloys proceeds via intermediate metastable phases. In SQ AlMg alloys the sequence and number of these phases depend on the ageing temperatures applied [15, 16]. For the precipitation below 323 K, the following sequence can apply (depending on the composition of the alloys studied)

$$\text{solid solution} \rightarrow \text{GP} (\rightarrow \beta'') \rightarrow \beta' \rightarrow \beta \quad (1)$$

where GP stands for Guinier–Preston zones, β'' is an intermediate phase, sometimes described as an ordered GP zone; probably having an $L1_2$ structure (Al_3Mg) [16], β' is a semi-coherent intermediate phase with a hexagonal unit cell ($a = 1.002$ nm and $c = 1.636$ nm [13]) and β is the equilibrium phase (about Al_3Mg_2) having an fcc unit cell ($a = 2.824$ nm [13]) that contains 1168 atoms.

The formation of the GP zones is associated with a large change in the enthalphy [2]. Thus, the GP-zone formation in LQ AlMg alloys can be traced by applying differential scanning calorimetry (DSC) [2]. It was found that the GP-zone formation in an LQ AlMg 12.8 at % alloy begun after a storage of 11.5 d at room temperature, whereas in an LQ AlMg 17.2 at % alloy it started after a storage of 3 d at room temperature. On annealing with constant rates between 5 and 40 K min^{-1}, the dissolution of GP zones was completed below 400 K [2]. According to Nozato and Ishihara [15] the dissolution temperatures of the GP and β'' zones, ranging from 330 to 360 K [15], do not strongly depend on the magnesium content of the alloys (magnesium contents between 7.5 and 12.5 at %). For the same alloys, the β' solvus probably lies between 500 and 550 K [15]. So, on ageing of quenched AlMg alloys at temperatures between 400 and 500 K, two basically different initial conditions can be discerned:

(i) the alloy contains GP zones formed during ageing at room temperature;

(ii) the alloy does not contain GP zones, because the ageing starts immediately after the quench.

In case (ii) a direct precipitation of the β' phase occurs.

The present study concerns the β'-precipitation process in LQ AlMg alloys with a magnesium content of 3.2, 10.5 and 16.7 at % by ageing at 404, 450

0022–2461/89 $03.00 + .12 © *1989 Chapman and Hall Ltd.*

and 492 K after a room-temperature storage varying between 27 and 970 d. So, case (i) holds for the specimens investigated (see above): a partial or a full development of GP zones has occurred during the room-temperature storage. However, it has been shown for case (i) that on annealing, the GP zones formed are always completely dissolved before any β'-phase precipitation starts [2]. Hence, in cases (i) and (ii) the β'-phase precipitation begins in an essentially single-phase matrix.

As dissolution of magnesium atoms in the aluminium matrix increases the aluminium-matrix lattice parameter, the precipitation of β' phase results in a decrease of the aluminium-matrix lattice parameter. Therefore, in this study the precipitation phenomena in LQ AlMg alloys were traced by the determination of the aluminium-matrix lattice parameter and its variance as derived from the X-ray diffraction line position and line broadening.

2. Experimental procedure

Aluminium alloys with an overall magnesium content of 3.2, 10.5 and 16.7 at % (the magnesium solid solubility at the eutectic temperature is 18.6 at % [17]) were prepared from 99.998 wt % Al and 99.99 wt % Mg. By the melt-spinning technique, ribbons with a thickness varying between 20 and 50 μm and a width of about 2 mm were obtained [18]. As deduced from dendrite-arm-spacing measurements, the cooling rate ranged from 10^6 to 10^7 K sec^{-1} [19]. After melt spinning, the ribbons were stored at room temperature for at least 27 d and for at most 970 d.

The aluminium-matrix lattice parameter was measured at room temperature as function of time of ageing in an oil bath maintained at 404 $\pm$ 4, 450 $\pm$ 2 or 492 $\pm$ 2 K. Parts cut from the ribbons were placed in a specimen holder that was used for the ageing treatment and that fitted in the Debye–Scherrer (DbS) camera, enabling investigation of the same sample throughout the whole ageing process. These specimen holders were placed in a specially designed heat-treatment cylinder pervious for oil, thereby protecting the vulnerable specimens. The temperature within the cylinder reached the temperature of the oil bath within 1 min. The aluminium-matrix lattice parameter values were obtained from DbS photographs – taken with Cu$K\alpha$ radiation and utilizing high-angle reflections – with a precision of 4 parts to 40 000. The values presented are valid at 298 K and were derived from the measured values by applying the appropriate thermal expansion coefficient [20].

The DbS photographs were also utilized to characterize the X-ray diffraction line broadening: with a densitometer the intensity on the equator of the DbS photographs was measured as a function of the diffraction angle. The Al {2 0 0} and the Al {2 2 0} line profile shapes of the LQ AlMg 10.5 at % and the LQ AlMg 16.7 at % alloys were determined, because these reflections yielded the line profiles with sufficient intensity at the highest possible diffraction angle. The background was interpolated linearly between the two extremities of the profiles obtained. The subsequent line-profile analysis was performed using the single-line Voigt technique [21].

3. Results

3.1. The shift of the aluminium-matrix reflections

The aluminium matrix lattice parameter is shown as a function of ageing time at the temperatures applied in Figs 1 and 2. The increase of the aluminium matrix lattice parameter occurring at the very start of ageing (see Fig. 2; note that the experimental error is about 4×10^{-5} nm) can be explained quantitatively by the annihilation of excess vacancies as discussed elsewhere [22].

The precipitation-induced decrease of the aluminium matrix lattice parameter occurs after an initial period with no measurable change of this lattice parameter. This period will be called the effective "incubation time". The effective incubation times for the LQ AlMg 16.7 at % alloy are shorter than those for the LQ AlMg

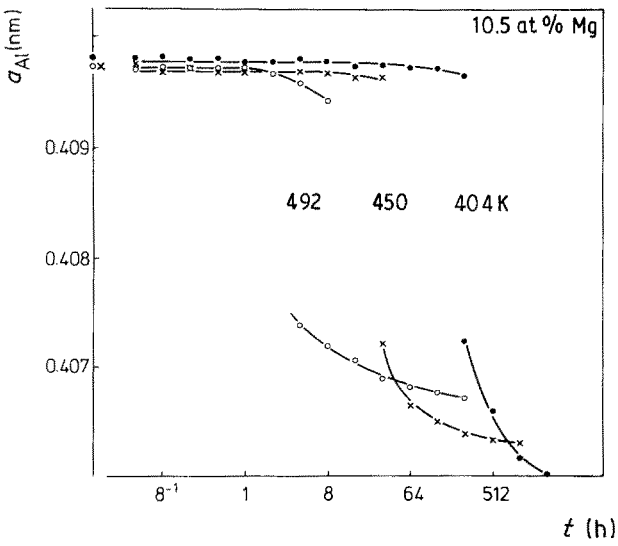

Figure 1 The aluminium matrix lattice parameter, a_{Al}, as a function of ageing time, t, for the LQ AlMg 10.5 at % alloy at the temperatures denoted.

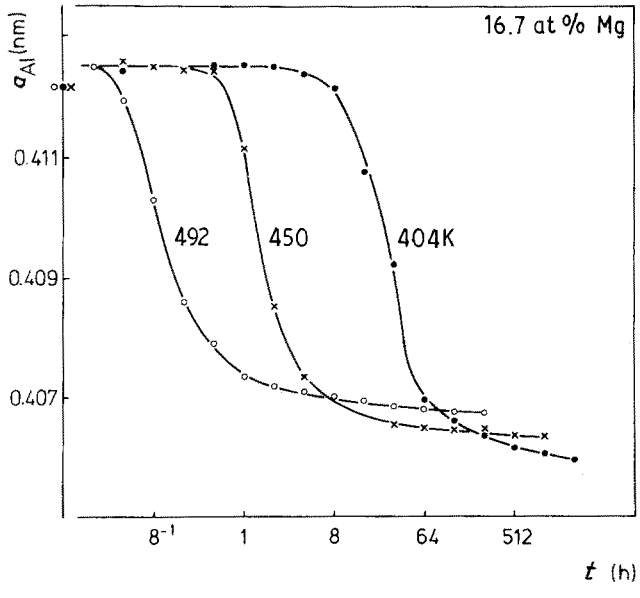

Figure 2 The aluminium matrix lattice parameter, a_{Al}, as a function of ageing time, t, for the LQ AlMg 16.7 at % alloy at the temperatures denoted (the values at $t = 0$ coincide).

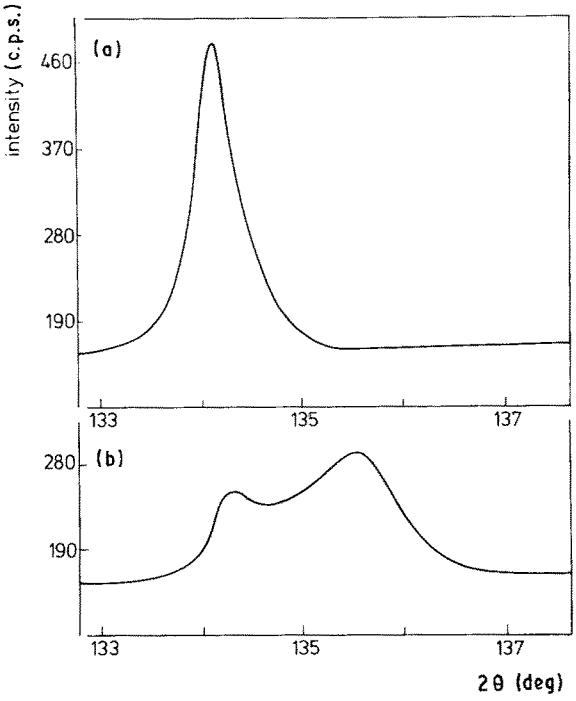

Figure 3 The Al {4 2 2} X-ray diffraction line profile as obtained from the LQ AlMg 10.5 at % alloy (a) as liquid quenched and (b) from the same alloy as aged for 4 h at 500 K. Line profiles were obtained by X-ray diffractometry using specimens prepared as described in [1] and applying Cu$K\alpha$ radiation; smoothing was performed and the α_2 component was eliminated.

10.5 at % alloy. For both alloys, the incubation time decreases with increasing ageing temperature.

The aluminium lattice parameter of the LQ AlMg 3.2 at % alloy does not show any indication of a precipitation-induced decrease on ageing at 404 ± 4 and 450 ± 2 K. Apparently no precipitation has occurred during the ageing times applied. Because the solid solubility at 492 K corresponds to the overall composition of the alloy [17], no precipitation can be expected in this alloy at 492 K.

The DbS photographs of the LQ AlMg 16.7 at % and the LQ AlMg 10.5 at % alloys obtained after 4 h ageing at 404 K and after 16 h ageing at 492 K, respectively, already exhibited diffraction lines that could be attributed to a hexagonal unit cell with an axial ratio, c/a, of about 1.68. This corresponds fairly well with the data given previously for the intermediate β'-phase [13]. No indication of the presence of diffraction lines corresponding to the equilibrium β- phase was obtained.

Remarkably, at the stage of precipitation where the overall rate of transformation is largest (Figs 1 and 2) the Al {4 2 2} and Al {3 3 3/5 1 1} line profiles from the LQ AlMg 10.5 at % alloy show two maxima (see Fig. 3, α_1 components only). This is interpreted as caused by the simultaneous presence of regions in the Al matrix at the beginning and at an advanced stage of magnesium-solute depletion. The behaviour of the lattice parameters calculated from the two intensity maxima is shown in Fig. 1 as a function of ageing time. A corresponding microstructure is shown in Fig. 4. No such effect could be observed for the LQ AlMg 16.7 at % alloy (see Section 4.1).

The progress of the magnesium depletion of a matrix

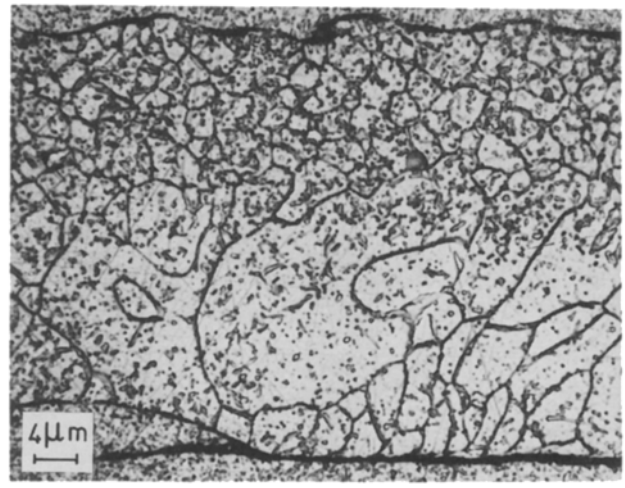

Figure 4 Optical micrograph of a cross-section of the LQ AlMg 10.5 at % alloy after 4 h ageing at 500 K, showing abundant precipitation at grain boundaries.

can be characterized (in the absence of macrostrains) by a precipitation/transformation parameter, 1-X_t, defined by

$$1 - X_t = \frac{c(t) - c(\infty)}{c(0) - c(\infty)} \simeq \frac{a_{Al}(t) - a_{Al}(\infty)}{a_{Al}(0) - a_{Al}(\infty)} \quad (2)$$

where $c(0)$, $c(t)$, $c(\infty)$ are the magnesium concentrations in the aluminium matrix and $a_{Al}(0)$, $a_{Al}(t)$, $a_{Al}(\infty)$ are the aluminium matrix lattice parameters at the start of ageing, after an ageing time, t, and in equilibrium, respectively. The equation $c = 4x/(a_{Al})^3$, with x as the atomic fraction of magnesium in solid solution relates the magnesium concentration, c, to the aluminium matrix lattice parameter, a_{Al}. Literature data have been used for the relation between x and a_{Al} [23–26] and for the equilibrium solid solubilities [17, 27]. In Figs 5 and 6, as derived from the intensity maxima observed for the aluminium matrix, $1 - X_t$ is shown as a function of ageing time at the temperatures indicated.

The equilibrium solid solubilities at the ageing temperatures applied, $x(\infty)$, correspond, within experimental error, to the values of x as derived from the values of the aluminium matrix lattice parameter measured after the largest ageing times at each temperature. This indicates a completed precipitation.

3.2. The broadening of the aluminium matrix reflections

X-ray diffraction line profiles are generally broadened by instrumental aberrations, the wavelength distribution and structural imperfections. The broadening by the instrumental aberrations and by the wavelength distribution can be determined by measuring corresponding line profiles from reference specimens. The reference specimen employed consisted of pure silicon powder (NBS SRM 640 (see [28]); 114 h annealed at 1473 K in an argon atmosphere). The breadth parameters characterizing the broadening of aluminium matrix reflections by instrumental aberrations and by the wavelength distribution were obtained by interpolation of data from, suitably chosen, measured line profiles of the reference specimen.

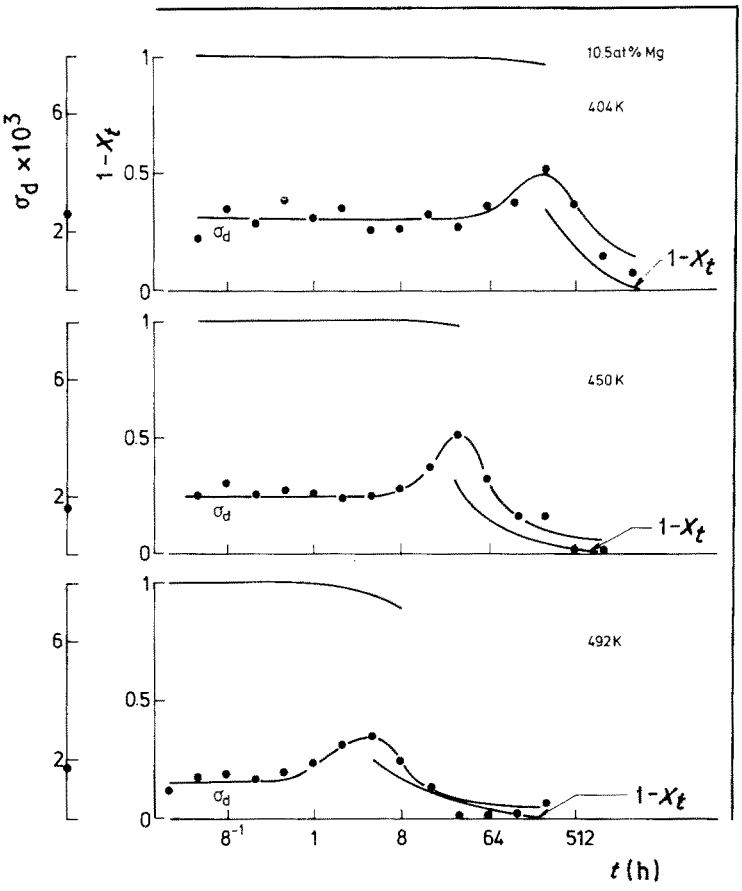

Figure 5 The fractional lattice-spacing variation σ_d in conjunction with the precipitation parameter $1-X_t$ as a function of ageing time, t, for the LQ AlMg 10.5 at % alloy at the temperatures denoted.

The line profile analysis was performed using the single-line Voigt method [21]. It is often assumed that the Gaussian component of the structurally broadened profile is dominated by lattice distortions, i.e. lattice-spacing variations and that the Cauchy component is mainly due to small domain sizes. It was found that the structurally broadened profile was nearly of Gaussian shape. Therefore, the total structural line broadening was interpreted as caused by lattice-spacing variations.

A parameter characterizing the width of the lattice spacing distribution can be obtained from the integral breadth, β^f, of the $h\,k\,l$ reflection after correction for instrumental aberrations, etc., as follows [21]

$$\sigma_d = \frac{\beta^f}{4 \tan \theta} \tag{3}$$

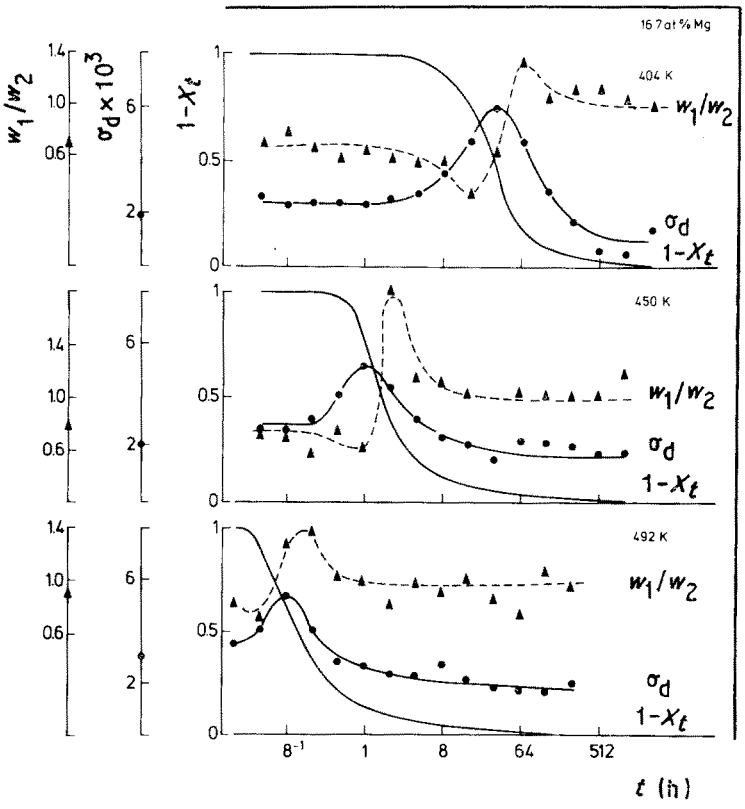

Figure 6 The fractional lattice-spacing variation σ_d and the ratio of the low-angle half-width, w_1, and the high-angle half-width, w_2, of the Al {2 2 0} line profile, w_1/w_2, in conjunction with the precipitation parameter $1-X_t$, as a function of ageing time, t, for the LQ AlMg 16.7 at % alloy at the temperatures denoted.

where θ is the Bragg angle. Values of the fractional lattice-spacing variation, σ_d, are shown in Figs 5 and 6 as a function of ageing time. Note, that the line broadening was measured for low-angle Bragg reflections where the instrumental resolution was insufficient to show doubly peaked reflections discussed for the LQ AlMg 10.5 at % alloy (high-angle reflections were of too low an intensity to allow accurate profile-shape determination, see Section 2, from DbS photographs). For the same times of ageing, the differences between σ_d values derived from the Al {2 0 0} and the Al{2 2 0} reflections are generally insignificant in view of the experimental inaccuracies. So, averaged data of σ_d only will be considered. The following observations can be made.

(i) For both alloys, σ_d remains constant during the effective incubation time; at the moment that the precipitation parameter $1 - X_t$ decreases, σ_d increases.

(ii) For the LQ AlMg 10.5 at % alloy, σ_d reaches a maximum at times where for $1 - X_t$ a high and a low value are observed simultaneously; for the LQ AlMg 16.7 at % alloy, σ_d reaches a maximum at times where the transformation proceeds fastest, i.e. for $1 - X_t \simeq 0.5$.

(iii) The maxima of σ_d are higher for the LQ AlMg 16.7 at % alloy than for the LQ AlMg 10.5 at % alloy.

(iv) On prolonged ageing, σ_d decreases until an approximately constant non-zero value is reached (see, in particular, the data for the LQ AlMg 16.7 at % alloy).

4. Discussion

4.1. Non-uniform precipitation

The observation of a pronounced line broadening, in association with the appearance of two intensity maxima in line profiles recorded from the LQ AlMg 10.5 at % alloy, is ascribed to the occurrence of significant compositional differences in the aluminium matrix during the transformation: the precipitation process takes place in a non-uniform manner (for detailed discussion of the line broadening, see Section 4.2.). In the past it was suggested that discontinuous precipitation (for terminology used, see the review given by Williams and Butler [29]), initiating heterogeneously at grain boundaries, could explain the appearance of two values for the aluminium-matrix lattice parameter [4, 5]; however, no microscopical evidence was presented. Instead, more recent transmission [10] and present transmission and scanning electron microscopy did not yield indications for the lamellar microstructure typifying the discontinuous precipitation reaction. However, the analysis of microstructure did reveal that abundant grain-boundary precipitation takes place in conjunction with precipitation in the bulk of the grains (see Fig. 4). Thus, it can be suggested that the difference in kinetics of grain-boundary and bulk precipitation leads to simultaneous occurrence of extended aluminium matrix regions adjacent to grain boundaries poor in magnesium solute and aluminium matrix regions in the bulk of the grains still rich in magnesium solute. Because the diffracted intensity is proportional to volume and the diffraction angle is related to composition (via the lattice spacing), the distribution of the intensity over the diffraction angle can be doubly peaked, as is seen in Fig. 3.

In a specimen, the bulk and the grain-boundary precipitation processes compete. If a high supersaturation of the aluminium matrix occurs, the bulk precipitation will dominate. Then a simultaneous occurrence of grain-boundary precipitation will not necessarily reveal itself by a distinct presence of a double aluminium matrix reflection, i.e. a single maximum occurs in the distribution of the intensity over the diffraction angle. This description apparently applies to the LQ AlMg 16.7 at % alloy, which has an initial solute supersaturation in the aluminium matrix much larger than the LQ AlMg 10.5 at % alloy.

An alternative explanation for the occurrence of additional diffraction maxima, especially at high Bragg angles, has been proposed by Gitgarts and Komarava [30]: elastic strains produced by the precipitation process "weaken the regular reflections and spread out the distribution of diffuse scattering" which would lead to complicated, multiply peaked total line profiles by superposition of the weakened normal and the diffuse scattering intensity distributions. With regard to this explanation the following remarks can be made.

1. In the present investigation, a doubly peaked reflection was only observed for the LQ AlMg 10.5 at % alloy during a very limited range of time where the overall change of $1 - X_t$ is half-way. For all other ageing times applied singly peaked reflections were observed.

2. For the ageing temperatures applied in [30] (comparable to those of this study) the doubly peaked reflections as observed here (the Al {4 2 2} and the Al {3 3 3/5 1 1} Cu$K\alpha$ profiles) cannot be detected in Fig. 1 of [30], possibly due to a relatively low angular resolution pertinent to the data given by those authors.

3. According to Gitgarts and Komarava [30], relaxation of the elastic strains would occur during prolonged ageing, implying a negligible line broadening remaining at the end of the ageing treatment. However, in this study a distinct line broadening is observed at the end of the ageing treatment, especially for the LQ AlMg 16.7 at % alloy (cf. Fig. 6). This remaining line broadening can be attributed to the elastic microstrains due to the misfit between the β'-phase precipitates and the aluminium matrix (see Section 4.2.).

In this paper it is thought that non-uniform precipitation explains the double maxima for aluminium matrix reflections observed during ageing of the LQ AlMg 10.5 at % alloy.

4.2. Line broadening during precipitation

Misfitting precipitates and compositional variations change lattice spacings. With respect to line broadening, two types of lattice-spacing variations can be distinguished:

(i) lattice-spacings variations within a coherently diffracting domain;

(ii) lattice-spacing differences between coherently diffracting domains.

Non-uniform precipitation is related to the occurrence of extended regions (domains) with different

average compositions and implies line broadening from origin (ii) mainly.

The line broadening related to non-uniform precipitation would reach its maximum when in one half of the specimen the precipitation has just been completed and in the other half no precipitation has occurred at all. Indeed, the maximal line broadening is observed at about half-way the overall change of $1 - X_f$.

The presence of line broadening of origin (ii) is also confirmed by the behaviour of w_1/w_2 on ageing, where w_1 and w_2 represent the low-angle and the high-angle half-widths of an X-ray diffraction line profile. In early stages of the precipitation process, magnesium solute-depleted regions of the matrix with a relatively small aluminium matrix lattice parameter are in the minority, implying for line broadening from origin (ii) a value of $w_1/w_2 < 1$, i.e. the line profile shows a high-angle tail. In later stages, a minor amount of the aluminium matrix is still rich in magnesium-solute atoms, implying for line broadening from origin (ii) a value of $w_1/w_2 > 1$, i.e. the line profile shows a low-angle tail. Such asymmetries can be pronounced in particular in the case of non-uniform precipitation. The ratio w_1/w_2 for the Al {2 2 0} reflection is plotted in Fig. 6 as a function of ageing time. It is observed that from the moment that precipitation becomes effective, the behaviour of the ratio w_1/w_2 corresponds to the foregoing discussion.

It should be noted that line broadening due to origin (i) will also be present during precipitation because of microstrains caused by the volume misfit between the precipitated semi-coherent β'-phase [13] and the aluminium matrix.

After liquid quenching, quenched-in stresses as well as compositional variations due to differences in solidification rates, e.g. between wheel- and upper sides of the ribbons, can occur [1, 31]. Hence, during the effective incubation time the observed line broadening is ascribed to such phenomena and thus can stem from origins (i) and (ii).

The maximum line broadening for the LQ AlMg 16.7 at % alloy is larger than for the LQ AlMg 10.5 at % alloy. This can be understood by considering the amount of β' phase to be precipitated: this amount is larger in the LQ AlMg 16.7 at % alloy than in the LQ AlMg 10.5 at % alloy; the volume-averaged misfit strains and compositional variations are larger in the LQ AlMg 16.7 at % alloy than in the LQ AlMg 10.5 at % alloy.

After completed precipitation all compositional variations have disappeared. Thereby, an important cause for asymmetry in the line profiles has been removed. The remaining line broadening is solely caused by the volume misfit between the β'-phase particles and the aluminium matrix, which appears to be associated with symmetrical line broadening with $w_1/w_2 = 1$ (see Fig. 6). Obviously, this remaining line broadening will be larger for the LQ AlMg 16.7 at % alloy than for the LQ AlMg 10.5 at % alloy (Figs 5 and 6).

4.3. β'-phase precipitation kinetics

By DSC analyses it was shown [2], that the GP/β'' zones were dissolved well below 400 K (see also Section 1), amply before any β' precipitation was detected. Because the ageing temperatures applied in this study lie between 400 and 500 K, it is assumed that a complete dissolution of the GP/β'' zones has occurred at the very start of the ageing treatment. Therefore, the effective incubation time for the β' precipitation, as indicated by the start of the decrease of the aluminium-matrix lattice parameter and by the increase of the line broadening, cannot be ascribed to GP/β'' dissolution.

In early stages of phase transformations the reaction rate can be controlled by two different activation energies, one for the formation of (critical) nuclei and the other for their subsequent growth [32]. In very many reactions the activation energy for nucleation decreases more than linearly with temperature, leading to a very rapid nucleation rate at large undercoolings, whereas the activation energy of growth is nearly independent of temperature [32]. Therefore, at sufficiently low temperatures the nucleation rate is so large, that the nucleation sites saturate very early in the reaction. Then, the activation energy for growth controls the overall reaction rate. It is suggested that this picture applies to the precipitation experiments of this study (maximal ageing temperature of 492 K). Consequently, the so-called effective incubation time is interpreted as a stage of such a low transformation rate that no measurable change of the aluminium matrix lattice parameter occurs (for example, Avrami kinetics with an Avrami exponent larger than 1 correspond to such a situation).

The stage of the precipitation process is characterized by the state variable kt, where t = the precipitation time and $k = k_0 \exp - E/k_B T_a$ with k_0 the pre-exponential factor, k_B Boltzmann's constant, T_a the ageing temperature and E the effective activation energy.

Supposing that after the effective incubation time, t_i, the same stage of the precipitation process has been reached, the activation energy during the time t_i can be deduced from the slope of the straight line obtained by plotting $\ln t_i$ (determined by the time until $1 - X_f = 0.998$) against $1/T_a$. For both alloys it is thus found to be (Fig. 7) $E = 0.7$ eV.

Growth of the β'-phase particles can occur via the migration of the substitutionally dissolved magnesium atoms through the aluminium matrix according to the vacancy mechanism. In the absence of excess vacancies, this transport of magnesium atoms will occur with an activation energy equal to about the sum of the migration and formation energies of a vacancy: ~ 1.3 eV [33]. The value found for the apparent activation energy is significantly smaller than 1.3 eV. This hints at the presence of excess vacancies retained after liquid quenching which effectively reduces the contribution of the vacancy-formation energy.

On liquid quenching, the predominant part of the excess vacancies will be gathered into vacancy loops [34–37]. At elevated temperatures (from 375 to 500 K) the excess vacancies collapsed into loops on liquid quenching are "reanimated" [37]: the vacancy loops emit vacancies assisting the β' precipitation. It is noted

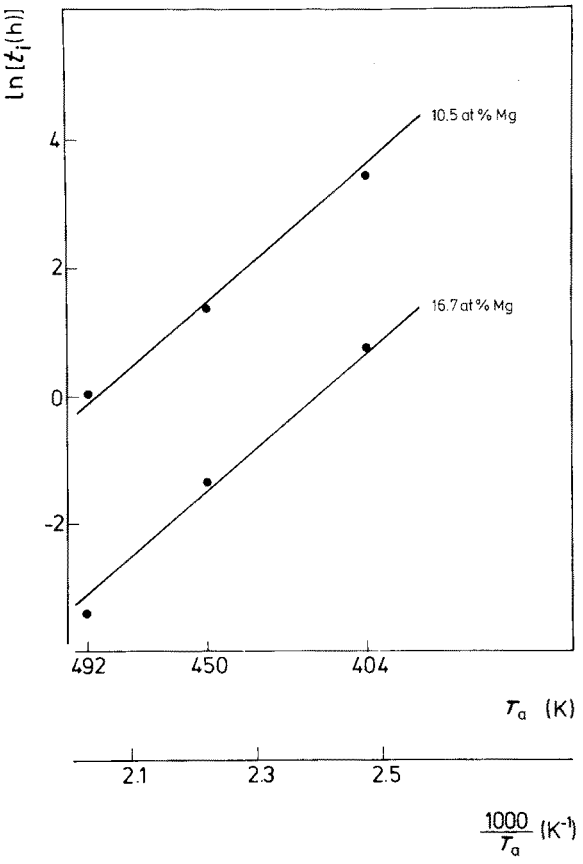

Figure 7 The value of the natural logarithm of the effective incubation time, t_i (taken as the time until $1\text{-}X_t = 0.998$) as a function of the reciprocal ageing temperature $1/T_a$ for the LQ AlMg alloys denoted.

that the same mechanism was adopted to explain the relatively low values of the activation energies for dissolution of GP zones in AlMg alloys [2] and for the precipitation of silicon in AlSi alloys [1].

5. Conclusions

1. In quenched AlMg alloys, non-uniform precipitation occurs: bulk and grain-boundary precipitation proceed at different rates.

2. The appearance of doubly peaked X-ray diffraction line profiles in association with pronounced, distinctly asymmetrical, line broadening is largely ascribed to appreciable compositional variations inherent to the non-uniform precipitation process.

3. The residual line broadening observed after the precipitation in the LQ AlMg alloys has been completed is caused by the elastic accommodation of the volume misfit between the β'-phase particles and the aluminium matrix.

4. The activation energy found for the initial β'-phase precipitation suggests strongly, that the kinetics of the β'-phase precipitation are governed by the growth of the precipitate particles via excess-vacancy enhanced volume diffusion of magnesium atoms.

Acknowledgements

Optical densitometer facilities were provided by Drs J. W. Visser and E. J. Sonneveld (Technisch-Physische Dienst TNO/TH, Delft). X-ray diffraction facilities were provided by Ing. N. M. van der Pers. Scanning electron microscopical analysis was performed by J. Toth (Centre for Submicron Technology, Delft University of Technology). Optical and electron transmission microscopy was performed by P. F. Colijn and C. D. de Haan, respectively. We are grateful to Professor B. M. Korevaar for stimulating discussions.

References

1. P. VAN MOURIK, E. J. MITTEMEIJER and T. H. DE KEIJSER, *J. Mater. Sci.* **18** (1983) 2706.
2. M. VAN ROOIJEN, J. A. SINTE MAARTENSDIJK and E. J. MITTEMEIJER, *Met. Trans.* AlgA (1988) 2433.
3. E. C. W. PERRYMAN and G. B. BROOK, *J. Inst. Metals* **79** (1951) 19.
4. MME. A. R. WEILL, *Rev. de Métallurgie* **XLIX** (1950) 364.
5. E. C. W. PERRYMAN, *Acta Metall.* **3** (1955) 412.
6. O. DAHL and K. DETERT, *Z. Metallkde* **46** (1955) 94.
7. S. MATSUO, *Trans. Nat. Res. Inst. Metals* **2** (1960) 22.
8. A. SAULNIER and P. MIRAND, *Mém. Rev. Métallurgie* **57** (1960) 91.
9. H. CORDIER and K. DETERT, *Z. Metallkde* **52** (1961) 321.
10. M. FELLER-KNIEPMEIER, K. DETERT and L. THOMAS, *ibid.* **55** (1964) 83.
11. J. D. EMBURY and R. B. NICHOLSON, *Acta Metall.* **11** (1963) 347.
12. A. DAUGER, J. P. GUILLOT and J. CAISSO, *Compt. Rend. Acad. Sci. Paris* **270** (1971) 915, série B.
13. M. BERNOLE, Thesis, University of Rouen (1974).
14. G. GAULT, Thesis, University of Limoges (1978).
15. R. NOZATO and S. ISHIHARA, *Trans. Jpn Inst. Metals* **21** (1980) 580.
16. K. OSAMURA and T. OGURA, *Metall. Trans. A* **15A** (1984) 835.
17. J. L. MURRAY, *Bull. Alloy Phase Diagr.* **3** (1982) 60.
18. A. BENDIJK, R. DELHEZ, L. KATGERMAN, T. H. DE KEIJSER, E. J. MITTEMEIJER and N. M. VAN DER PERS, *J. Mater. Sci.* **15** (1980) 2803.
19. M. VAN ROOIJEN, N. M. VAN DER PERS, L. KATGERMAN, T. H. DE KEIJSER and E. J. MITTEMEIJER, in Proceedings of the 5th International Conference on Rapidly Quenched Metals, 1985, edited by S. Steeb and H. Warlimont (North Holland, Amsterdam, 1985) p. 823.
20. E. J. MITTEMEIJER, P. VAN MOURIK and T. H. DE KEIJSER, *Phil. Mag. A* **43A** (1981) 1157.
21. T. H. DE KEIJSER, J. I. LANGFORD, E. J. MITTEMEIJER and A. B. P. VOGELS, *J. Appl. Crystallogr.* **15** (1982) 308.
22. P. VAN MOURIK, T. H. DE KEIJSER and E. J. MITTEMEIJER, in Proceedings of the 5th International Conference on Rapidly Quenched Metals, 1985, edited by S. Steeb and H. Warlimont (North Holland, Amsterdam, 1985) p. 899.
23. D. M. POOLE and H. J. AXON, *J. Inst. Metals* **80** (1951–1952) 599.
24. B. C. ELLWOOD, *ibid.* **80** (1951–1952) 605.
25. J. E. DORN, P. PIETROWSKY and T. E. TIETZ, *Trans. AIME* **188** (1950) 933.
26. W. J. HELFRICH and R. A. DODD, *ibid.* **224** (1962) 757.
27. L. F. MONDOLFO "Aluminium Alloys; Structure and Properties" (Butterworths, London, 1976) p. 313.
28. C. R. HUBBARD, H. E. SWANSON and F. A. MAUER, *J. Appl. Crystallogr.* **8** (1975) 45.
29. D. B. WILLIAMS and E. P. BUTLER, *Int. Met. Rev.* **26** (1981) 153.
30. M. J. GITGARTS and V. I. KOMARAVA, *Phys. Met. Metall.* **53** (1982) 170.
31. J. A. VAN DER HOEVEN, P. VAN MOURIK and E. J. MITTEMEIJER, *J. Mater. Sci. Lett.* **2** (1983) 158.
32. J. W. CHRISTIAN, "The Theory of Transformations in Metals and Alloys", 2nd Edn (Pergamon, Oxford, 1975) p. 543.
33. R. W. SIEGEL, *J. Nucl. Mater.* **69/70** (1970) 117.

34. P. B. HIRSCH, J. SILCOX, R. E. SMALLMAN and K. H. WESTMACOTT, *Phil. Mag.* **3** (1958) 897.
35. D. KUHLMANN-WILSDORF and H. G. F. WILSDORF, *J. Appl. Phys.* **31** (1960) 516.
36. M. KIRITANI, *J. Phys. Soc. Jpn* **20** (1965) 1834.
37. E. OZAWA and H. KIMURA, *Mater. Sci. Engng* **8** (1971) 327.

Received 15 September 1988
and accepted 10 January 1989